Multiple input/output waveguides light-induced by a single Bessel beam for all-optical interconnects

Yue Chai, Nacera Bouldja, Nicolas Marsal, Delphine Wolfersberger

Multiple inputs/outputs waveguides light-induced by a single Bessel beam for all-optical interconnects

YUE CHAI,[1,2,*] NACERA BOULDJA,[1,2] NICOLAS MARSAL,[1,2] AND DELPHINE WOLFERSBERGER[1,2]

[1] *Université de Lorraine, CentraleSupélec, LMOPS, F-57000 Metz, France*
[2] *Chair in Photonics, CentraleSupélec, LMOPS, F-57070 Metz, France*
[*] *yue.chai@centralesupelec.fr*

Abstract: We numerically study photo-induced waveguides using a single Bessel beam in a photorefractive (PR) medium. Under self-focusing nonlinearity, we demonstrate the possibility for creating complex waveguiding structures with multiple inputs/outputs channels. The truncation of the incoming Bessel beam, the nonlinearity of the PR medium, the light intensity, the order and the size of the Bessel beam are the key parameters for achieving different configurations with high guiding efficiencies. As such not only classical X or Y couplers but also more complex structures can be generated with up to 7 identified inputs/outputs. These results provide large opportunities for all-optical interconnects.

1. Introduction

Optical interconnects is an active branch of research for the optical community with several applications ranging from information storage, optical computing or future intelligent networks [1]. Compared to the electrical interconnections, it offers advantages such as broad bandwidths, high-speed transmission, low cross-talk independent of data rates and high interconnect densities. For that, several technologies, including silicon waveguide crossings [2], optical fibers, photonic components, photonic integrated circuits have been proposed [3]. However, those classical optical systems necessarily work with high peak power, and they are usually bulky, passive, and not reconfigurable.

In order to overcome the previous shortcomings, alternative approaches for creating reconfigurable complex waveguiding structures have been developed. One of the most widespread approach is based on photo-induced waveguides using either Kerr or Photorefractive effect to artificially design index structures inside a nonlinear material [4–6]. For example, a laser beam propagating in bias PR crystal may excite free charge carriers to create an internal electric field through drift and diffusion effects [7]. This so called space charge field induces through the Pockels effect a refractive index distribution in the medium. This latter permits the creation of reconfigurable waveguiding structures through the intensity distribution of the incoming light beam. Usually, self-trapping of classical Gaussian beams [4–6] are used for such a photo-induced inscription. More recently, unconventional beams for example with Airy profile became also a potential solution for the induction of complex waveguiding structures in nonlinear media. Under strong focusing nonlinearity, such a self-accelerating, diffraction-free, multi-lobes profile and their interactions can induce complex waveguiding structures offering multiple inputs/outputs channels [8–13].

Among the unconventional beams family, Bessel, Mathieu, and Weber beams have been generated and studied [14]. In 2012, P.A.Sanchez-Serrano et al. developed a genetic algorithm to generate these beams [15]. In addition to the three types of unconventional beams above, they also generated more complex nondiffractive beams with this algorithm, such as an asymmetric Bessel

beam, cosine-like beams that bent periodically in a zigzag pattern and a spiral beam. Going back to the Bessel profile, it was first proposed by Durnin in 1987 [16] and has been studied most extensively, especially because of its nondiffracting characteristic [17]. Experimentally, the Bessel beam has to be truncated by a Gaussian term [18]. As such it propagates diffraction-free in a finite distance and has self-healing ability in free space [19, 20]. Because of these properties, Bessel beams have been studied in several domains for example in free-space optical interconnects [21], for reconfigurable photo-induced networks [22], in light localization induced by Bessel photonic lattices [23] and more generally for all-optical switching [24]. Moreover, it is worth noting that in a nonlinear medium, the propagation of Bessel beam exhibits a self-trapping and a breather-forming behavior under self-focusing conditions [25, 26]. Thanks to the previous phenomena, F. Xin et al. demonstrated the possibility to photo-induce multiwaveguiding structures using several weakly diffracting Bessel beams in a quadratic nonlinear medium [27].

In this paper, we numerically demonstrate that a single self-focusing Bessel beam propagating in a PR medium can induce complex waveguiding structures with multiple inputs and outputs. We show that these waveguides are reconfigurable by changing the system parameters such as the waist of the Gaussian envelop, the nonlinearity of the PR crystal, the power, the order, and the size of the Bessel beam. To test the efficiency of the photo-induced structures, we numerically propagate one or two Gaussian beams through the different waveguide inputs. We observe that the probe beams are guided linearly along the photo-induced trajectories and may split into multiple output gates. By comparing to previous works using Airy beams propagation [10, 12] and analyzing the energy guiding efficiency and the distance between the different outputs channels, we show more complex guiding configurations, addressing up to 7 outputs, with high guiding efficiency and a more important distance shift between the different outputs.

2. Numerical Model

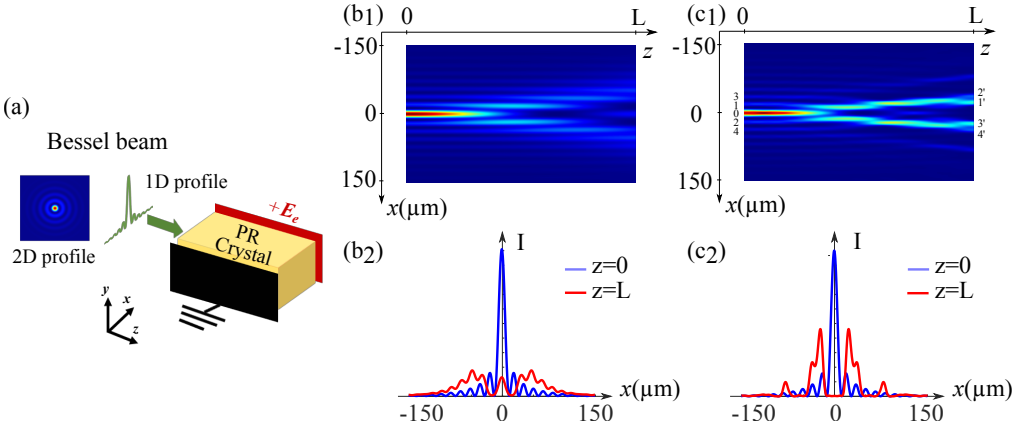

Fig. 1. (a) Scheme of principle for the injection of Bessel beams in a PR crystal (length $L = 1\ cm$). (b_1) Normalized intensity distribution of a 1D-single zero-order Bessel beam ($x_0 = 10\ \mu m$, $\omega_0 = 150\ \mu m$, $F_0 = \sqrt{25}$) with linear propagation ($\Gamma = 0$) in the PR crystal. (c_1) Normalized intensity distribution of the 1D-single zero-order Bessel beam ($x_0 = 10\ \mu m$, $\omega_0 = 150\ \mu m$, $F_0 = \sqrt{25}$) with nonlinear propagation ($\Gamma = 3$) in the PR crystal. (b_2) and (c_2) Transverse intensity profiles corresponding respectively to (b_1) and (c_1).

The typical scheme of a Bessel beam propagating in a biased PR crystal is illustrated in [Fig. 1(a)]. In the following, we consider only the case of a 1D-Bessel beam injection. The normalized profile of the incident Bessel beam electric field F is defined mathematically as:

$$F(X, Z = 0) = F_0 J_n(X) \exp(-\frac{X^2}{(\omega_0 \cdot k_t)^2}), \tag{1}$$

where J is the Bessel function with n its related order, F_0 is the maximum electric field amplitude of the Bessel beam, $X = k_t x = 2x/x_0$ is the normalized transverse coordinate with x_0 the waist of the main lobe of the zero-order Bessel beam and k_t the transverse wave number which is related to the beam size with the relation of $x_0 = 2/k_t$, $Z = z/L_d$ is the propagating length normalized by $L_d = kx_0^2/2$, which is the Rayleigh length of the separated central lobe of the zero-order Bessel beam, k is the wave number [25], and ω_0 is the waist of the Gaussian truncated term. The equation describing the nonlinear propagation of the Bessel beam along the Z-axis is given by:

$$i\partial_Z F + \partial_X^2 F = \Gamma E_0 F, \tag{2}$$

In this expression, Γ, $n_0 = 2.3$, r_{eff} represent respectively the nonlinearity strength, the linear refractive index, and the electro-optical coefficient of the PR crystal. $\Gamma = \frac{k^2}{k_t^2} n_0^2 r_{eff} E_e$ and $E_0 = E_{sc}/E_e$ is the normalized space charge field where E_e is the applied external electrical field and E_{sc} is the space charge field induced by the drift and diffusion effects in the crystal [7]. The temporal evolution of this normalized space charge field is calculated by a relaxation-type dynamics given by

$$\tau \partial_t E_0 + E_0 = -\frac{I}{(1 + I)}, \tag{3}$$

where $\tau = \tau_0/(1 + I)$ is the relaxation time of the crystal, τ_0 is the characteristic response time of the PR crystal, and $I = |F|^2$ is the normalized total intensity [28].

3. Results and Discussion

In the following, we simulated numerically Eq.(2) by the Fast Fourier Transform Beam Propagation Method (FFTBPM) similar to [10]. With this method, we solve in the real space the nonlinear guiding effect along the propagation direction (Z) by using a classical beam propagation method, then the diffraction effects in the transverse directions (X) are solved in the Fourier space by using the fast Fourier transform. It is worth stressing that all the following results concern the stationary state in which the final caluclated total intensity remains fixed when time increases after a transient duration, pictures are therefore taken after a time loop duration equals to 20τ.

We first consider a zero-order Bessel beam with $x_0 = 10\ \mu m$, $\omega_0 = 150\ \mu m$, $F_0 = \sqrt{25}$ ($\Gamma = 0$) propagating linearly in the PR crystal of length $L = 1\ cm$. Figures 1(b_1), 1(b_2) show respectively the intensity distribution and the transverse profiles of the Bessel beam on each side of the PR crystal [input side (blue line) and output side (red line)]. We observe the linear propagation and diffraction of this truncated Bessel beam at the output of the crystal with a diffraction length $L_D \approx 5mm$.

Then we study the waveguiding structure achieved by the same Bessel beam propagating in the 1 cm PR crystal with a nonlinearity $\Gamma = 3$ in the (+z)-direction. Figures 1(c_1), 1(c_2) show the intensity distribution and the corresponding transverses profiles. The numbers $(0, 1, 2, 3, 4)$ are respectively the positions corresponding to the main central lobe and the first four side lobes of the incoming Bessel beam. Under the Pockels effect, the Bessel beam is self-focused and the nonlinearity compensates its diffraction. Therefore, the corresponding refractive index change induces two well separated waveguide outputs at positions $(1', 3')$ and two other less intense nearby outputs at positions $(2', 4')$ at the crystal face $z = L$ [Figs. 1(c_1) and 1(c_2)].

To analyze the guiding efficiency of this configuration, we consider the refractive index variation constant and fixed by keeping the final result of the normalized space charge field distribution E_0 calculated by Eq.3. Then we inject Gaussian probe beams into different positions

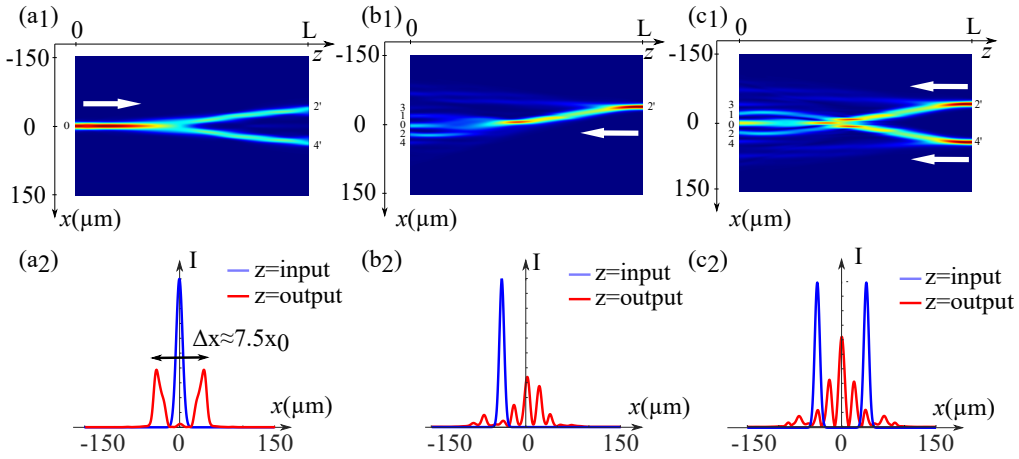

Fig. 2. Test of the configuration shown in figure 1(c_1) ($x_0 = 10\ \mu m$, $\omega_0 = 150\ \mu m$, $F_0 = \sqrt{25}$, $\Gamma = 3$). (a_1), (b_1), (c_1) Normalized intensity distributions of the Gaussian probe beams propagating linearly in the photo-induced waveguiding structure. (a_2), (b_2), (c_2) Inputs and outputs transverse profiles when the Gaussian probe beams propagate respectively from 0 to $(2', 4')$, $2'$ to $(0, 1, 2)$, and $(2', 4')$ to $(0, 1, 2, 3, 4)$.

with high refractive index changes and calculate their propagations under linear conditions. Figures 2(a_1), 2(b_1), 2(c_1) show the propagating intensity patterns of the probe beams and figures 2(a_2), 2(b_2), 2(c_2) illustrate the corresponding inputs (blue line) at the front face of the crystal and outputs (red line) profiles at the back face. It is worth mentioning that only the outputs of more than 10% of the maximum input probe beam intensity are of interest for optical interconnects applications [29]. Thus, in the following, only outputs fulfilling this condition will be studied.

As shown in [Figs. 2(a_1) and 2(a_2)], when we inject a Gaussian beam in the position 0, it linearly propagates in the (+z)-direction (as indicated by the white arrow). Two outputs with the same intensity peak are observed at $(2', 4')$. The output profile in [Fig. 2(a_2)] shows that the structure can guide 76% of the input energy (38% for each output of this "Y" coupler). This results is more efficient than the similar one presented in [10] induced by a single Airy beam. Moreover, compared to [10], the distance between two output positions is larger with Bessel beams $\Delta x \approx 7.5 x_0$ offering easiest solutions for addressing applications.

We also decided to test the opposite situation where the Gaussian probe beam injected in $2'$ at $z = L$ propagates to (-z)-direction. Figures 2(b_1), 2(b_2) show that three outputs with peak intensities of 33%, 27%, 15% respectively at $(0, 1, 2)$ can be addressed. Owing to the symmetrical structure of the induced configuration shown in [Fig.1(c_1)], when the same probe beam is injected in $4'$ instead of $2'$, the same demultiplexing structure with three outputs at $(0, 1, 2)$ is induced. We therefore proposed to inject simultaneously two incoherent Gaussian beams into the two symmetrical positions $(2', 4')$. As shown in [Figs. 2(c_1) and 2(c_2)] the beams first gather then split into five outputs at $(0, 1, 2, 3, 4)$. These results can be achieved because of the high refractive index structure induced by the intrinsic side lobes distribution of the Bessel beam.

On this basis, to further specify the influence of the intrinsic side lobes, we discuss the influence of the Gaussian envelope parameter ω_0, which specifies the side lobes number and intensity of the incoming Bessel beam. Thus, we consider two zero-order Bessel beams with $x_0 = 10\ \mu m$ (same characteristics as the incoming Bessel beam in [Fig. 1(c_1) and 1(c_2)]) but with respectively higher truncation ($\omega_0 = 50\ \mu m$) and weaker truncation ($\omega_0 = 250\ \mu m$) with $\Gamma = 3$ (same as in the previous configuration). Figures 3(a_1), 3(a_2) show the intensity distribution

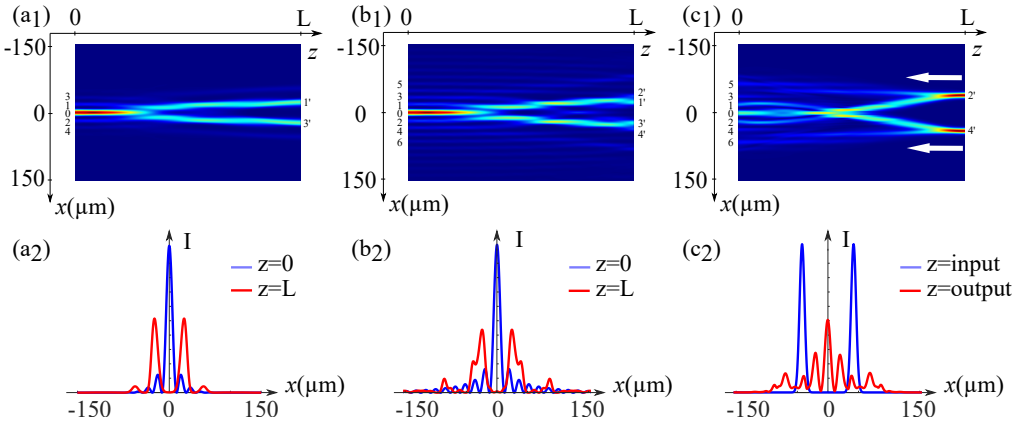

Fig. 3. (a_1) Normalized intensity distribution of the strong truncated zero-order Bessel beam ($x_0 = 10\ \mu m$, $\omega_0 = 50\ \mu m$, $F_0 = \sqrt{25}$) with nonlinear propagation ($\Gamma = 3$) in the PR crystal.(a_2) transverse profile of the Bessel beam corresponding to (a_1). (b_1) Normalized intensity distribution of the little truncated zero-order Bessel beam ($x_0 = 10\ \mu m$, $\omega_0 = 250\ \mu m$, $F_0 = \sqrt{25}$) with nonlinear propagation ($\Gamma = 3$) in the PR crystal.(b_2) transverse profile of the Bessel beam corresponding to (b_1).(c_1) Normalized intensity distribution of probe beam linearly propagating in the waveguide structure induced by (b_1). (c_2) input and output profiles corresponding to (c_1).

and transverse profiles achieved by the Bessel beam with $\omega_0 = 50\ \mu m$. As illustrated in [Fig. 3(a_2), input profile (blue line)], the highly truncated Bessel beam has only six side lobes, and each of them is less intense than that at the same position shown in [Fig. 1(c_2), input profile (blue line)]. Consequently, comparing [Fig.3(a_1) and 3(a_2)] to [Fig.1(c_1) and 1(c_2)], for a highly truncated Bessel beam ($\omega_0 = 50\ \mu m$), although a high self-focusing arises under nonlinear conditions, the waveguiding structure presents fewer channels. Likewise, figures 3(b_1), 3(b_2) show the intensity distribution and the transverse profiles of the propagation of the Bessel beam with $\omega_0 = 250\ \mu m$. We add the numbers $(5, 6)$ which are respectively the two symmetrical positions corresponding to the fourth side lobes on both sides of the central lobe. For this case, we do the same guiding test as that in [Fig.2 (c_1)] and compare them. When we inject two Gaussian beams into the positions $(2', 4')$ as shown in [Fig.3(c_1)], two more outputs with more than 10% ($\approx 12.8\%$) of the maximum input probe beam intensity are observed at $(5, 6)$. The more intense side lobes can induce a higher refractive index variation in the writing process so that the corresponding waveguiding channels can transmit more energy. Thus, it is possible to obtain more guiding channels by using a less truncated Bessel beam. In conclusion, the above simulation and discussion about the truncation parameter demonstrate that varying ω_0 would be an efficient way to control the number of channels for the waveguiding structures.

As our optical platform possess several control parameters, we now investigate the previous configurations for higher value of the nonlinearity. This parameter can be modified either by changing the nonlinear coefficient strength (Γ) either increasing the intensity of the incident Bessel beam (F_0) or applying a higher external electric field E_e. In what follows, we study the waveguiding structure by only increasing Γ up to 6 and F_0 up to $\sqrt{36}$. Under these new conditions, figure 4(a_1) shows a channel with a more intense refractive index change in the center. Comparing with the results in [Fig. 1(c_1)], by increasing the nonlinear strength in the crystal, the stronger focusing effect induces a soliton-like configuration [Fig. 4(a_1)], which localized the refractive index changes toward the center instead of splitting this latter into two branches like in [Fig. 1(c_1)]. We now inject a Gaussian beam in $0'$ and transmit it towards (-z)-direction as indicated by the white arrow in [Fig. 4(b_1)]. Interestingly, the probe beam splits now into three outputs

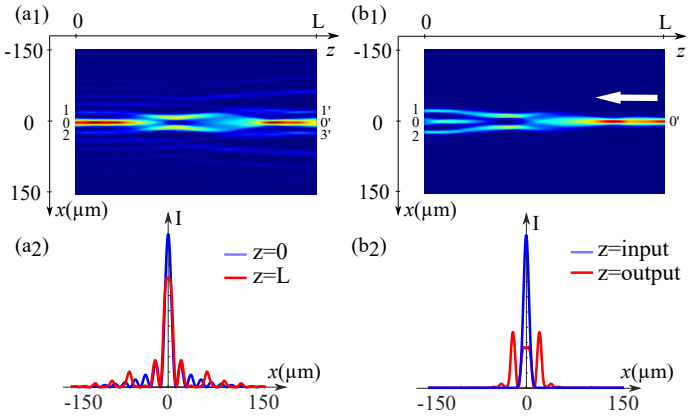

Fig. 4. Waveguiding structures induced by the zero-order Bessel beam in a PR crystal with higher nonlinearity ($x_0 = 10\ \mu m$, $\omega_0 = 150\ \mu m$, $F_0 = \sqrt{36}$, $\Gamma = 6$, $L = 1\ cm$). (a_1) Normalized intensity distribution. (a_2) transverse profile of the Bessel beam in both side of crystal. (b_1) Normalized intensity distribution of probe beam linearly propagating in the waveguide structure. (b_2) input and output transverse profiles corresponding to (b_1).

of more than 25% of the total incoming intensity at $(0, 1, 2)$ (corresponding positions of main lobe and the first two side lobes of the Bessel beam). Such a feature brings more possibilities of photo-induced waveguiding structures such as new optical interconnect schemes with one input and three outputs.

So far, we demonstrated that our system based on a zero-order Bessel beam photo-induced waveguiding structures can be used and reconfigured as a Y coupler, a demultiplexer with one input and three outputs or a waveguide with two inputs and seven outputs. It is worth mentioning that our Bessel beam based platform yield more possibilities that cannot be achieved with one Gaussian beam. Nevertheless, similar demultiplexing structures with multiple outputs could be formed by spatial solitons only induced by multiple Gaussian beams [30].

All the previous cases focused on a zero-order Bessel beam and the influence of the nonlinearity in the PR crystal on the induced waveguiding configurations. As presented in [31], the Bessel beam profile depends on the order of the Bessel function. It is worth noting that a higher order Bessel beam has a dark spot in the center and the size of this dark spot increases with the order number. We therefore decided to study the scenario where waveguiding structures are induced by higher order Bessel functions [a second-order Bessel beam ($n = 2$)]. In addition to the influence of the beam shape itself on the light-induced waveguiding structures, we study the impact of the beam size based on the second-order Bessel beam.

We first inject a second-order Bessel beam ($n = 2$) with $x_0 = 11\ \mu m (k_t = 0.18\ \mu m^{-1})$, $\omega_0 = 150\ \mu m$, $F_0 = \sqrt{4}$ into a 1 cm PR crystal with $\Gamma = 6$. Figures 5(a_1), 5(a_2) show the intensity distribution and the profiles at both sides of the crystal. In [Fig. 5(a_1)], we notice that no light is present in the center of the intensity distribution and the self-focusing lobes create a waveguiding structure with multiple parallel channels. To test this structure, we inject two incoherent Gaussian probe beams and transmit them to the (+z)-direction. Figures 5(b_1), 5(b_2) show the intensity distribution during the propagation of the probe beams and the normalized intensity profile of input and output probe beams. It shows that the probe beams gather and then split into two outputs on $(1', 3')$ with identical peak intensity. This X coupler scheme can only be achieved by a high-order Bessel beam by taking advantage of its two lobes with identical intensity beside the dark spot in the center. Interestingly, when we inject the probe beams in $(1', 3')$ and linearly transmit them to the other side of the crystal (direction indicated by the white arrow), the beams

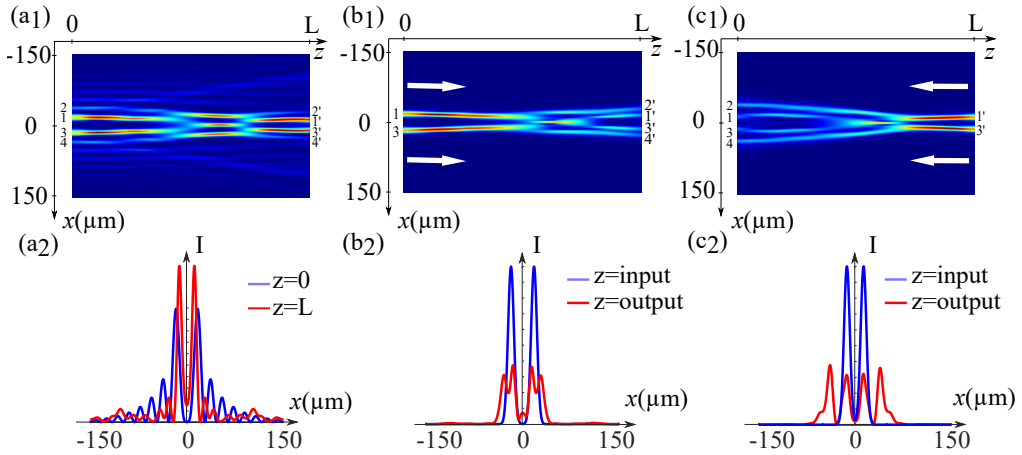

Fig. 5. Waveguiding structures induced by a second-order Bessel beam function in a biased PR crystal ($x_0 = 11\ \mu m, k_t = 0.18\ \mu m^{-1}, \omega_0 = 150\ \mu m, F_0 = \sqrt{4}, \Gamma = 6, L = 1\ cm$). ($a_1$) Normalized intensity distribution, (a_2) transverse profile of the Bessel beam in both sides of crystal. (b_1) Normalized intensity distribution of test beam propagating from $(1, 3)$ to $(1', 2', 3', 4')$, (b_2) corresponding input and output profiles. (c_1) Normalized intensity distribution of test beam propagating from $(1', 3')$ to $(1, 2, 3, 4)$. (c_2) Corresponding input and output profiles.

propagate differently. Figures 5(c_1), 5(c_2) plot the intensity distribution and corresponding beam profiles in this case. As shown, the probe beams first gather and evenly split into four outputs $(1, 2, 3, 4)$ with the same intensity.

Now, we focus on the waveguiding structures by varying the size of the incident second-order Bessel beam, thus indirectly changing the diffraction length of the Bessel beam. As mentioned in [32], the Bessel beam can be decomposed by a set of planes waves propagating on a cone. The opening angle of this cone, which defines the size of the Bessel beam center core, is related to the ratio of the transverse wave number to the longitudinal wave number. Thus, the Bessel beam size can be changed by only varying the transverse wave number k_t as we defined the relation $x_0 = 2/k_t$ in the previous section referring to the numerical model. Figures 6(a_1), 6(a_2) show the induced waveguiding structure and the corresponding profiles in the case of $k_t = 0.15\ \mu m^{-1}$. Comparing the incident Bessel beam profile (blue line) in [Fig. 6(a_2)] to that shown in [Fig. 5(a_2)], we see that the lobes next to $x = 0$ in [Figs. 6(a_1) and 6(a_2)] are farther apart [the distance between two principal lobes in [Fig. 6(a_2)] (41 μm) is about 7 μm larger than that in [Fig. 5(a_2)] (33.4 μm)], and the waist of these lobes is larger [the waist of the principal lobe in [Fig.6(a_2)] (11.5 μm) is about 2.5 μm larger than that in [Fig.5(a_2)] (9 μm)]. Because of the diffraction which becomes smaller for higher beam waist, we can observe in [Figs. 6(a_1) and 6(a_2)] that the waveguiding structure has shifted to the right compared to [Fig. 5 (a_2)] and three output gates are now addressable on the output side of the crystal. Similarly to [Fig. 5(b_1) and 5(b_2)], we inject two Gaussian beams in the left side of the crystal in channels $(1, 3)$ to $(0', 1', 2')$. As illustrated in [Figs. 6 (b_1) and 6(b_2)], we are able to guide two probe beams into three outputs with similar high intensities. Finally, if we inject the Gaussian beams in $(1', 2')$ and guide them to the (-z)-direction, the beams split into four outputs located on $(1, 2, 3, 4)$ as shown in [Figs. 6(c_1) and 6(c_2)]. Note that those located on $(1, 3)$ have more intensities than those shown in [Fig. 5(c_2)] due to the greater injection distance between two probe beams. This can be explained by less energy losses when two more separated probe beams split directly without any interaction during their propagation.

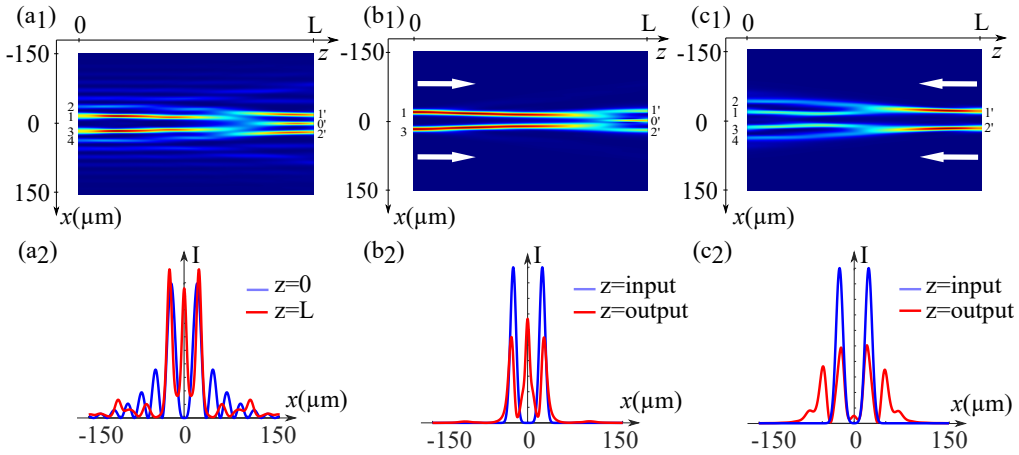

Fig. 6. Waveguiding structures induced by the second-order Bessel beam with $x_0 = 13.5\mu m (k_t = 0.15\mu m^{-1})$ in a biased PR crystal ($\omega_0 = 150\ \mu m$, $F_0 = \sqrt{4}$, $\Gamma = 6$, $L = 1cm$). (a_1) Normalized intensity distribution. (a_2) Corresponding transverse profile of the Bessel beam in both sides of the crystal. (b_1), (b_2) Normalized intensity distributions and input/output profiles of Gaussian probe beams propagating from $(1, 3)$ to $(0', 1', 2')$. (c_1), (c_2) Normalized intensity distributions and input/output profiles of Gaussian probe beams propagating from $(1', 2')$ to $(1, 2, 3, 4)$.

4. Conclusion

In conclusion, we have analyzed numerically the optical waveguide configurations formed by a single Bessel beam in a PR medium and analyzed their guiding features. We demonstrate that these photo-induced waveguiding structures can be used and reconfigured as a Y coupler, a demultiplexer with one input and three outputs or a multiple-coupler with two inputs and seven outputs. Those multiple inputs and outputs have better coupling efficiency than those created by several Gaussians [4, 30] or a single Airy beam [10]. For example, the Y-coupler with one input and two outputs induced by the single zero-order Bessel beam presents a guiding efficiency of 76% of the total intensity compared to 50% of that induced by the single Airy beam [10]. Moreover, by changing the parameters, such as the waist of the Gaussian envelop, the nonlinearity in the crystal (via the input beam intensity or the external applied electric field), the incident Bessel beam's order, and the size parameter, we can control the number of active channels and consequently enlarge the optical interconnects possibilities. Under higher self-trapping effect, zero-order Bessel beam induces soliton-like configuration so that it can be used as one input to three outputs components. For a second-order Bessel beam, thanks to its profile without any bright lobe in the center, an efficient symmetrical complex waveguiding structure with two inputs and four outputs can be photo-induced. Finally, in a more general situation where most of the experiments are in 2+1D, it is worth noting that the Bessel beam involves a two-dimensional profile in the transverse (x,y) plane and that the anisotropic response of the nonlinear medium through drift and diffusion effects should be taken into account in the generation of the space charge field [33, 34]. Regardless, as mentioned in [28, 35], the same model could be used for phenomenological predictions in a 2+1D configuration. Our numerical simulations motivate therefore future experimental investigations for optical interconnects in all-optical communication and information processing applications.

Funding. Chair in Photonics; Region Grand Est; GDI Simulation; Departement de la Moselle; European Regional Development Fund (ERDF); CentraleSupélec; Fondation CentraleSupélec; Metz Metropole; China Scholarship Council (CSC).

Disclosures. The authors declare no conflicts of interest.

Data availability. Data underlying the results presented in this paper are not publicly available at this time but may be obtained from the authors upon reasonable request.

References

1. S. Aleksic, "The future of optical interconnects for data centers: A review of technology trends," in *2017 14th ConTEL,* (IEEE, 2017), pp. 41–46.
2. S. Wu, X. Mu, L. Cheng, S. Mao, and H. Fu, "State-of-the-art and perspectives on silicon waveguide crossings: A review," Micromachines **11**, 326 (2020).
3. D. Tsiokos and G. Kanellos, "Optical interconnects: fundamentals," in *Optical Interconnects for Data Centers,* (Elsevier, 2017), pp. 43–73.
4. J. Petter, C. Denz, A. Stepken, and F. Kaiser, "Anisotropic waveguides induced by photorefractive (2+ 1) d solitons," J. Opt. Soc. Am. B **19**, 1145–1149 (2002).
5. S. Lan, M.-f. Shih, and M. Segev, "Self-trapping of one-dimensional and two-dimensional optical beams and induced waveguides in photorefractive knbo 3," Opt. Lett. **22**, 1467–1469 (1997).
6. M.-f. Shih, M. Segev, and G. Salamo, "Circular waveguides induced by two-dimensional bright steady-state photorefractive spatial screening solitons," Opt. Lett. **21**, 931–934 (1996).
7. N. Kukhtarev, V. Markov, S. Odulov, M. Soskin, and V. Vinetskii, "Holographic storage in electrooptic crystals.: I. steady state," in *Landmark Papers On Photorefractive Nonlinear Optics,* (World Scientific, 1995), pp. 37–48.
8. T. Bouchet, N. Marsal, M. Sciamanna, and D. Wolfersberger, "Solitonic characteristics of airy beam nonlinear propagation," Phys Rev A **97**, 051801 (2018).
9. N. Wiersma, N. Marsal, M. Sciamanna, and D. Wolfersberger, "Airy beam self-focusing in a photorefractive medium," Sci. Rep. **6**, 35078 (2016).
10. N. Wiersma, N. Marsal, M. Sciamanna, and D. Wolfersberger, "All-optical interconnects using airy beams," Opt. Lett. **39**, 5997–6000 (2014).
11. P. Rose, F. Diebel, M. Boguslawski, and C. Denz, "Airy beam induced optical routing," Appl. Phys. Lett. **102**, 101101 (2013).
12. T. Bouchet, N. Marsal, M. Sciamanna, and D. Wolfersberger, "Light-induced interconnects using nonlinear airy beam interactions," JPhys Photonics **1**, 025001 (2019).
13. N. Marsal, N. Wiersma, M. Sciamanna, and D. Wolfersberger, "Counterpropagating interactions of self-focusing airy beams," Sci. Rep. **9**, 1–6 (2019).
14. J. C. Gutiérrez-Vega, M. Iturbe-Castillo, and S. Chávez-Cerda, "Alternative formulation for invariant optical fields: Mathieu beams," Opt. Lett. **25**, 1493–1495 (2000).
15. P. A. Sanchez-Serrano, D. Wong-Campos, S. Lopez-Aguayo, and J. C. Gutiérrez-Vega, "Engineering of nondiffracting beams with genetic algorithms," Opt. letters **37**, 5040–5042 (2012).
16. J. Durnin, "Exact solutions for nondiffracting beams. i. the scalar theory," J. Opt. Soc. Am. A **4**, 651–654 (1987).
17. J. Durnin, J. Miceli Jr, and J. Eberly, "Diffraction-free beams," Phys. Rev. Lett. **58**, 1499 (1987).
18. F. Gori, G. Guattari, and C. Padovani, "Bessel-gauss beams," Opt. Commun. **64**, 491–495 (1987).
19. R. MacDonald, S. Boothroyd, T. Okamoto, J. Chrostowski, and B. Syrett, "Interboard optical data distribution by bessel beam shadowing," Opt. Commun. **122**, 169–177 (1996).
20. Z. Bouchal, J. Wagner, and M. Chlup, "Self-reconstruction of a distorted nondiffracting beam," Opt. Commun. **151**, 207–211 (1998).
21. N. K. Alababneh, "Bessel beams and gaussian beams as information carriers in free space optical interconnects systems: a comparison study," Int. J. Electr. Comput. Eng. **9**, 3488 (2019).
22. Z. Xu, Y. V. Kartashov, and L. Torner, "Reconfigurable soliton networks optically-induced by arrays of nondiffracting bessel beams," Opt. Express **13**, 1774–1779 (2005).
23. R. Fischer, D. N. Neshev, S. López-Aguayo, A. S. Desyatnikov, A. A. Sukhorukov, W. Krolikowski, and Y. S. Kivshar, "Light localization in azimuthally modulated bessel photonic lattices," J. Mater. Sci. Mater. Electron. **18**, 277–283 (2007).
24. F. Diebel, D. Leykam, M. Boguslawski, P. Rose, C. Denz, and A. S. Desyatnikov, "All-optical switching in optically induced nonlinear waveguide couplers," Appl. Phys. Lett. **104**, 261111 (2014).
25. R. Gadonas, V. Jarutis, R. Paškauskas, V. Smilgevičius, A. Stabinis, and V. Vaičaitis, "Self-action of bessel beam in nonlinear medium," Opt. Commun. **196**, 309–316 (2001).
26. M. Flammini, G. Di Domenico, D. Pierangeli, F. Di Mei, A. J. Agranat, and E. DelRe, "Observation of bessel-beam self-trapping," Phys. Rev. A **98**, 033808 (2018).
27. F. Xin, M. Flammini, F. Di Mei, L. Falsi, D. Pierangeli, A. J. Agranat, and E. DelRe, "Using bessel beams to induce optical waveguides," Phys. Rev. Appl. **11**, 024011 (2019).
28. M. Belić, P. Jander, K. Motzek, A. Desyatnikov, D. Jović, A. Strinić, M. Petrović, C. Denz, and F. Kaiser, "Counterpropagating self-trapped beams in photorefractive crystals," J. Opt. B: Quantum Semiclassical Opt. **6**, S190 (2004).
29. N. Wiersma, "Photorefractive self-focusing of airy beams : nonlinear interactions and all-optical waveguiding," Ph.D. thesis, Université de Lorraine (2016).

30. V. Coda, M. Chauvet, F. Pettazzi, and E. Fazio, "3-d integrated optical interconnect induced by self-focused beam," Electron. Lett. **42**, 463–465 (2006).
31. D. S. Simon, *A Guided Tour of Light Beams: From lasers to optical knots*, 2053-2571 (Morgan & Claypool Publishers, 2016).
32. D. McGloin and K. Dholakia, "Bessel beams: diffraction in a new light," Contemp. Phys. **46**, 15–28 (2005).
33. E. DelRe, A. Ciattoni, and A. J. Agranat, "Anisotropic charge displacement supporting isolated photorefractive optical needles," Opt. Lett. **26**, 908–910 (2001).
34. E. DelRe, G. De Masi, A. Ciattoni, and E. Palange, "Pairing space-charge field conditions with self-guiding for the attainment of circular symmetry in photorefractive solitons," Appl. Phys. Lett. **85**, 5499–5501 (2004).
35. M. Petrović, D. Jović, M. Belić, J. Schröder, P. Jander, and C. Denz, "Two dimensional counterpropagating spatial solitons in photorefractive crystals," Phys. review letters **95**, 053901 (2005).